Supporting Information

Eu^{3+} Sensitization via Nonradiative Interparticle Energy Transfer Using Inorganic Nanoparticles

Marie Anne van de Haar[*1], Anne C. Berends[1], Michael R. Krames[1,3], Liudmyla Chepyga[2], Freddy T. Rabouw[2], Andries Meijerink[2]*

[1]Seaborough Research BV, Matrix VII Innovation Center, Science Park 106, Amsterdam, The Netherlands

[2]Utrecht University, Princetonplein 1, 3584 CC Utrecht, The Netherlands

[3]Arkesso LLC, 2625 Middlefield Rd, No 687, CA 94306, Palo Alto, California, USA

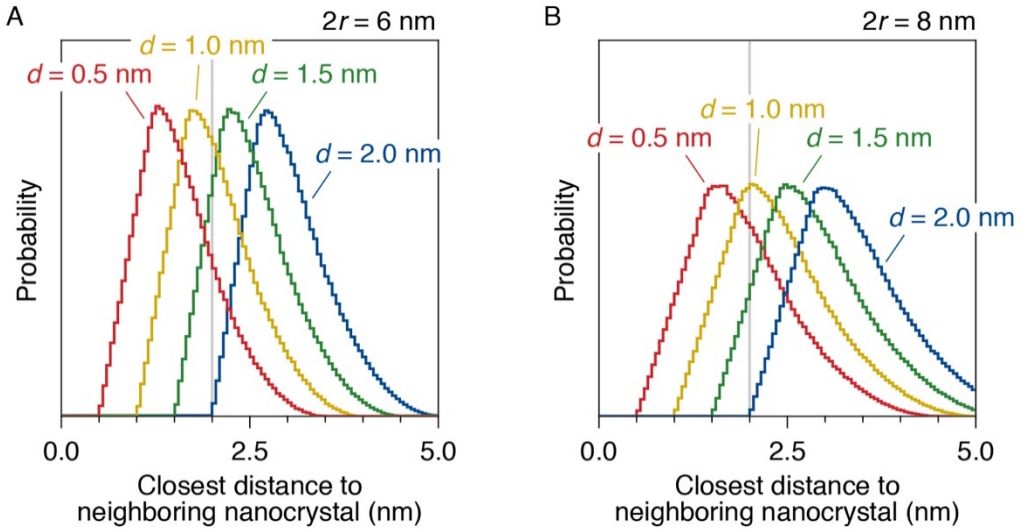

Figure S1. The distribution of closest distances to a neighboring NC in a close-packed NC film calculated with respect to locations within a central NC. We consider NC films with face-centered cubic packing, with NC radii of (a) 2r = 6 nm and (b) 2r = 8 nm, and surface-to-surface separations between the NCs of d = 0.5 (red), 1.0 (yellow), 1.5 (green), and 2.0 nm (blue). The simulation algorithm Monte Carlo generates 10^6 random locations within a central NC per curve and then calculates the closest distance to a neighboring NC. The curves shown are histograms of these closest distances. We see that in principle the distribution of distances is tunable by controlling the NC diameter and, through surface chemistry, the NC separation. With the right choice of parameters, e.g. 2r = 6 nm and d = 1.0 nm, the majority of sensitizer ions in a central NCs are situated within 2 nm of a neighboring NC. The distribution of distances translates into a distribution of IFRET rates, which is further tunable with the ratio of sensitizer and emitter NCs in the NC film and with the doping concentration in the emitter NCs. Alternatively, high doping concentration in the sensitizer NCs would enable intra-particle energy migration as a pathway that connects sensitizer ions in the center of the NC with those on the surface. This could further increase the efficiency of IFRET.

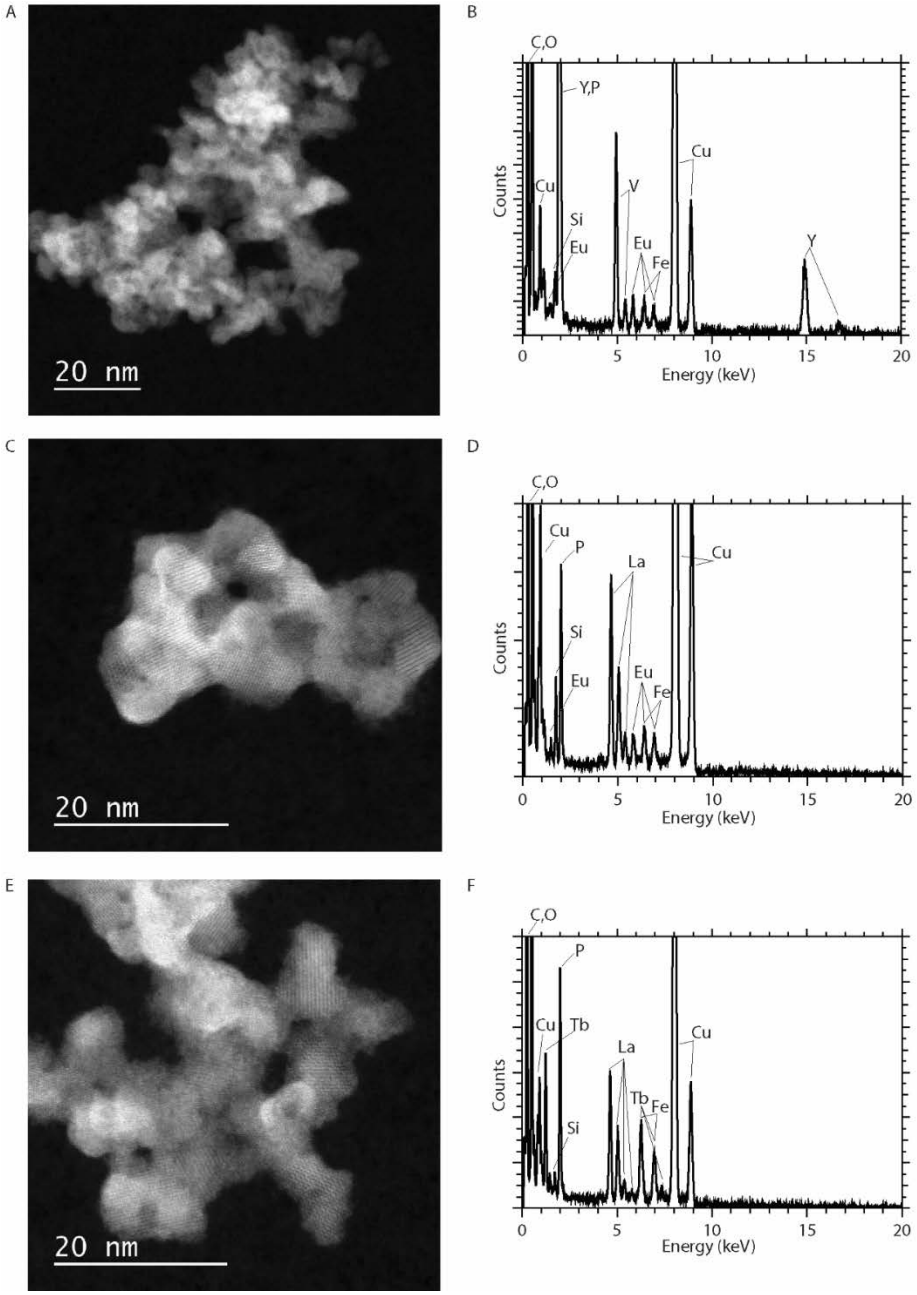

Figure S2. (a,c,e) HAADF-STEM images and (b,d,f) STEM-EDX spectra of the entire clusters visualized in the corresponding STEM images. (a,b) $YVPO_4$:Eu, (c,d) $LaPO_4$:Eu, and (e,f) $LaPO_4$:Tb NCs after ligand removal. Individual NC sizes are sub-10 nm, but tightly clustered together due to the ligand removal. EDX analysis show all expected elements. Cu, Fe and Co originate from the used TEM grid and the objective lens, respectively.

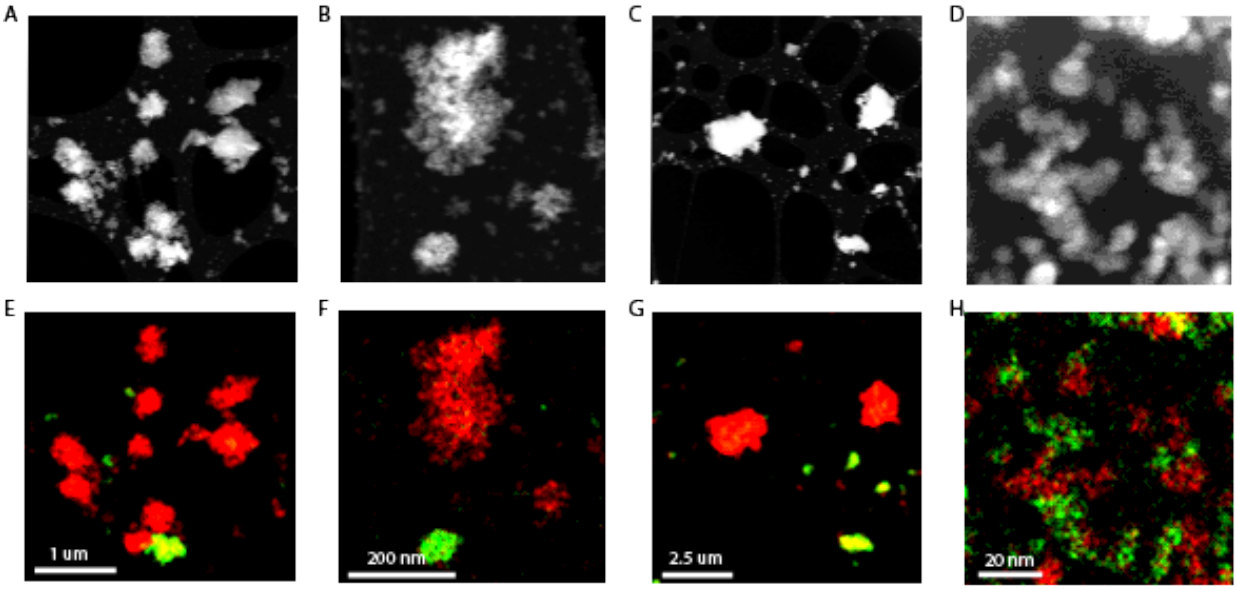

Figure S3. (a-d) HAADF-STEM images and (e-h) TEM-EDX map of (a,b,c,e,f,g) dry mixed, and (d,h) wet mixed $LaPO_4$:Tb / $YVPO_4$:Eu NCs on different scales. Green represents lanthanum (in $LaPO_4$:Tb), red represents vanadium (in $YVPO_4$:Eu). Ligands have been removed before imaging.

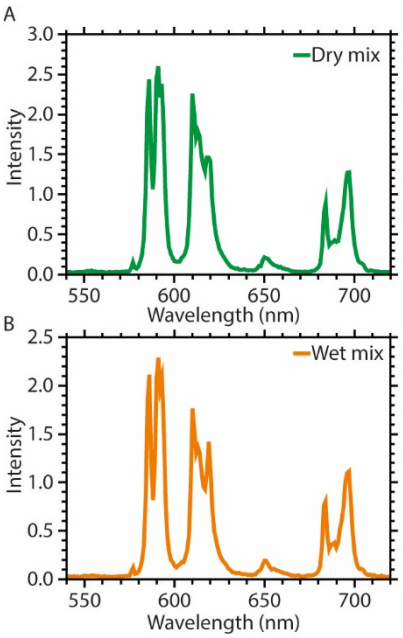

Figure S4. Emission spectra upon direct Eu^{3+} excitation at λ = 395 nm, of (a) dry mixed and (b) wet mixed $LaPO_4$:Tb / $LaPO_4$:Eu NCs measured under identical conditions. Both spectra show a similar Eu^{3+} emission intensity.

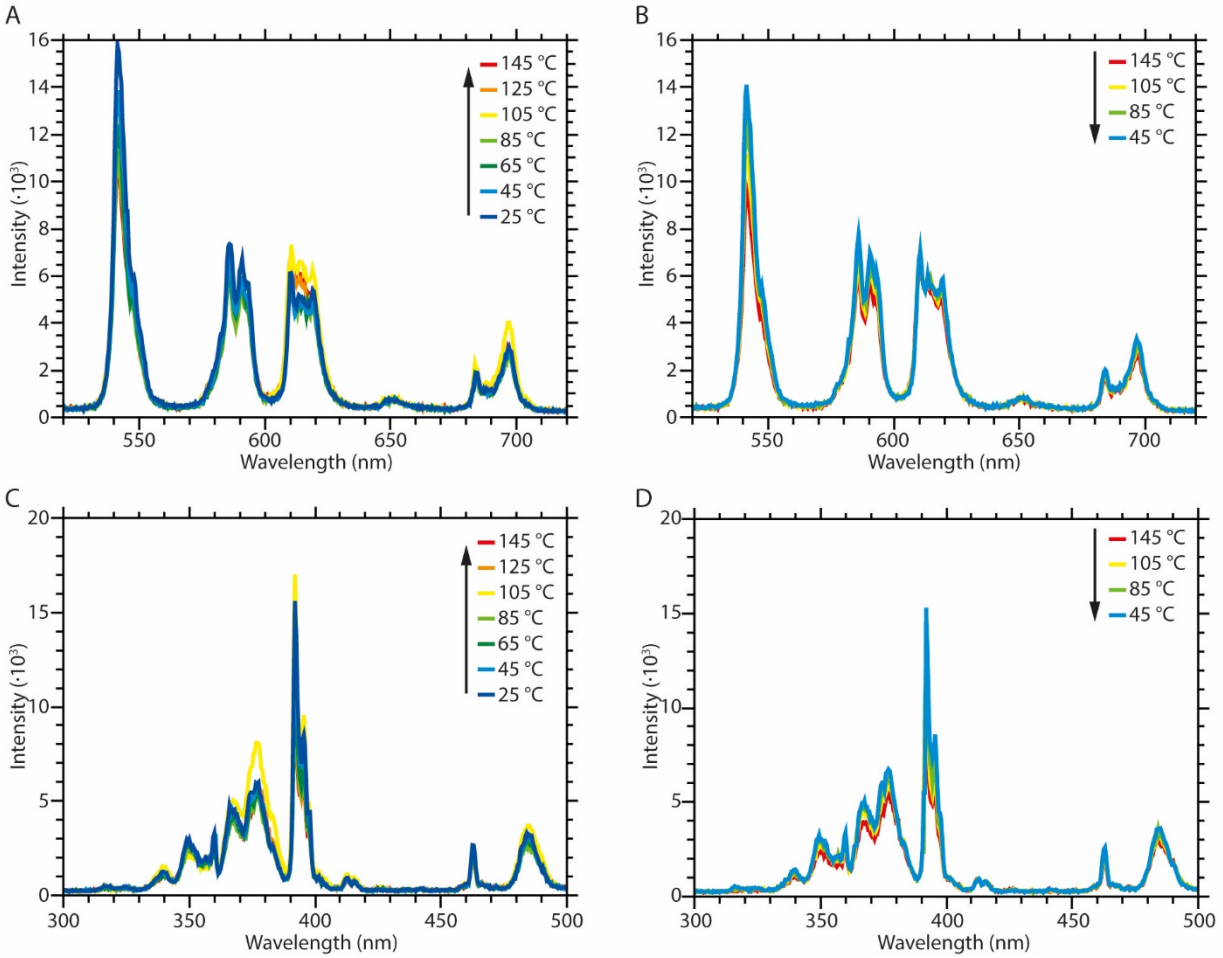

Figure S5. Temperature dependent (a,b) emission and (c,d) excitation spectra on wet mixed $LaPO_4$:Tb / $LaPO_4$:Eu NCs. For (a,c) spectra are recorded while gradually increasing the temperature, whereas for (b,d) spectra are measured upon cooling the sample. Both emission and excitation spectra show reversible behavior of the emission quenching at elevated temperatures.

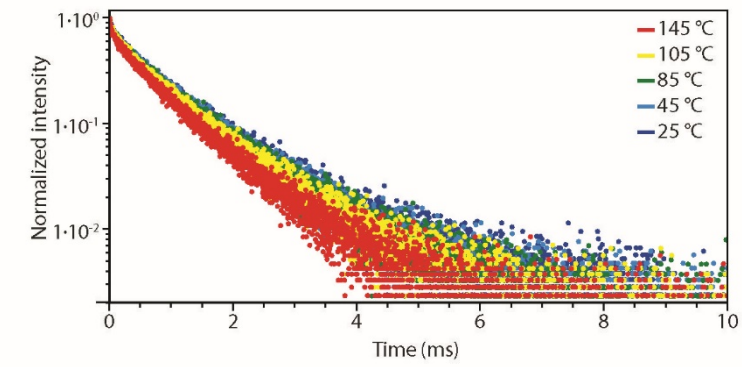

Figure S6. Photoluminescence decay curves of the Tb^{3+} $^5D_4$ emission in wet-mixed $LaPO_4$:Tb/$LaPO_4$:Eu NC composites, measured at different temperatures. Excitation at λ = 484.5 nm, emission was monitored at λ = 542 nm. A slight acceleration of the decay is observed at higher temperatures in line with slightly increased ET rates which could explain the stability of the Eu^{3+} emission at elevated temperatures. However, the decay behavior reflects a complex interplay between IFRET and other non-radiative effects, especially at higher temperatures.

Further research is needed to draw more reliable conclusions from the luminescence decay curves.

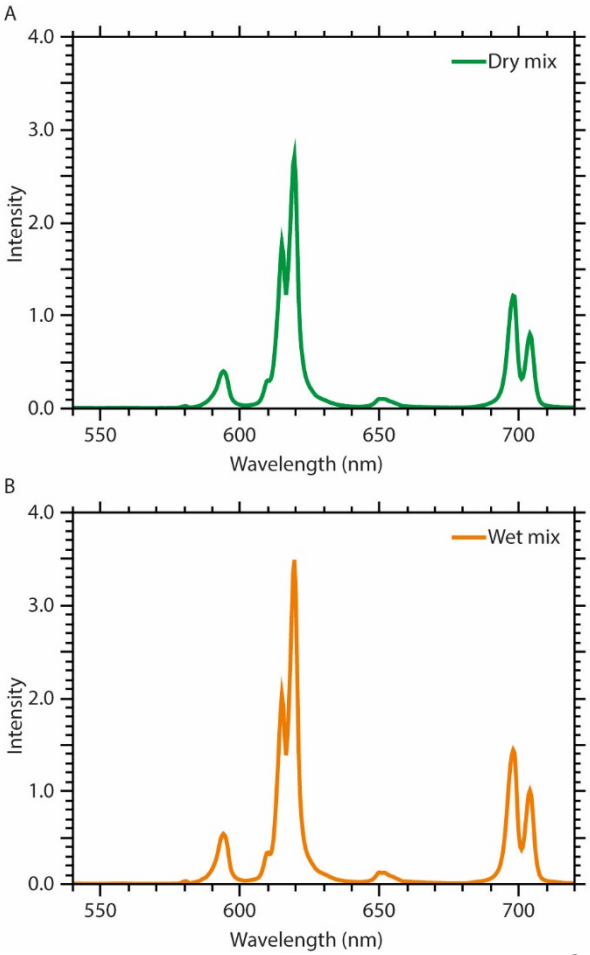

Figure S7. Emission spectra upon direct Eu^{3+} excitation at λ = 395 nm, of (a) dry mixed and (b) wet mixed $LaPO_4$:Tb / $YVPO_4$:Eu NCs. The wet mixed NCs show a slightly higher Eu^{3+} emission intensity compared to the dry mixed NCs, but the difference is much smaller compared to the difference in Eu^{3+} emission intensity when excited at λ = 484.5 nm (see Fig. Figure 7b in the main text).

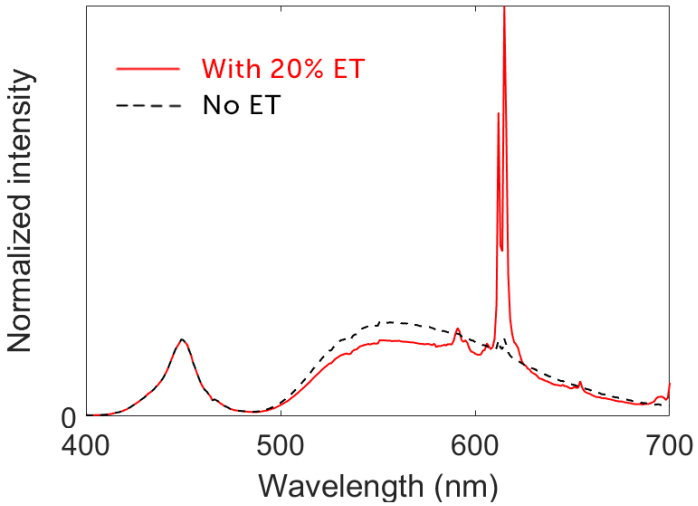

Figure S8. Simulated white LED spectra with 20% (red solid line) and without (black dotted line) IFRET. A blue LED with a 450 nm peak wavelength was used as blue emitter, $Y_3Al_5O_{12}$:Ce was used as green emitter. Energy transfer efficiencies in the order of only 20% are sufficient to achieve white light.

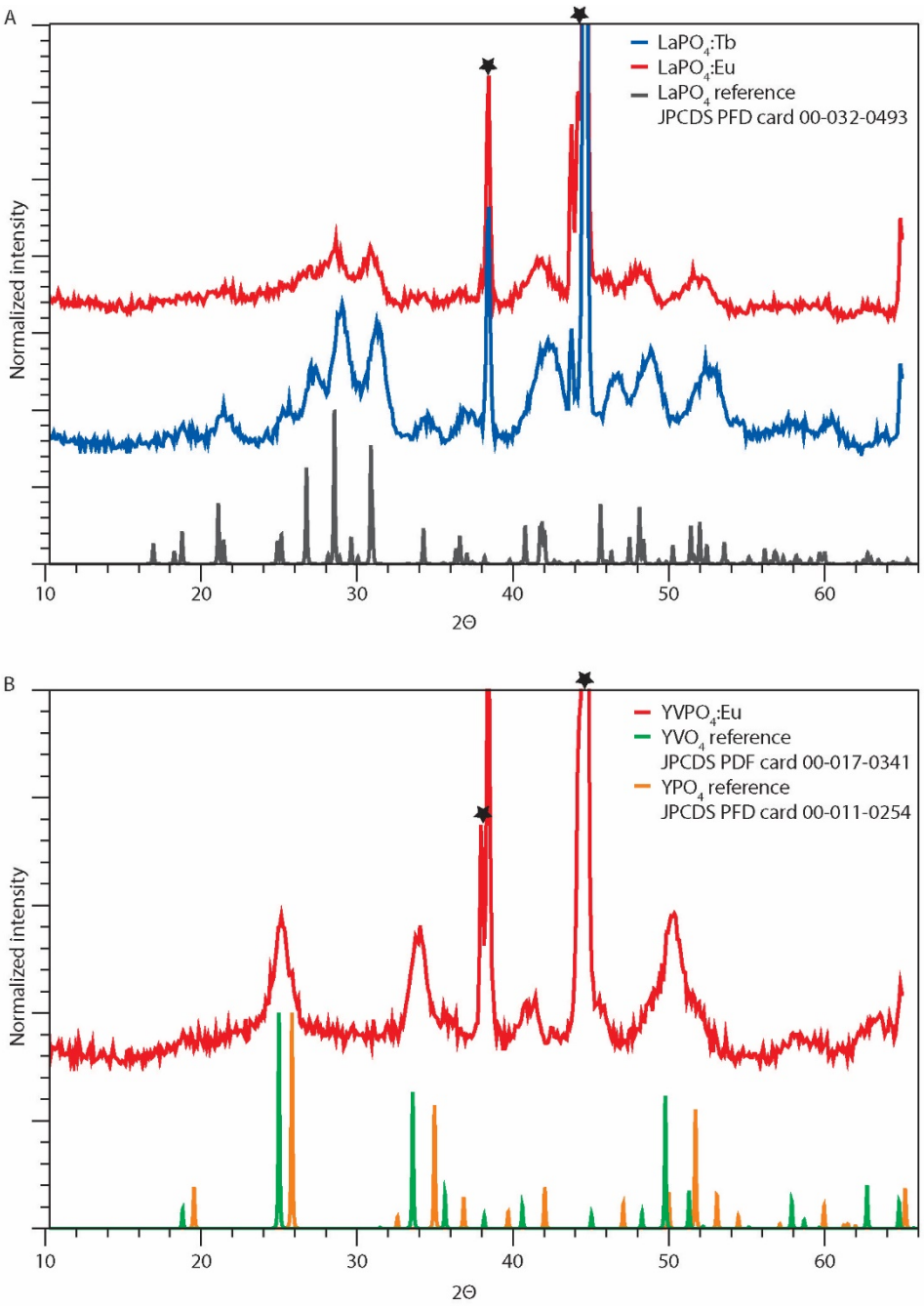

Figure S9. XRD patterns for (a) $LaPO_4$:Eu and $LaPO_4$:Tb, and (b) $YVPO_4$:Eu. All peaks in the measured diffractograms match the displayed reference data (YPO_4 and YVO_4 for the $YVPO_4$:Eu nanocrystals, as the mixed $(VP)O_4$ material was not available). Broadening of the peaks is due to the small size of the nanocrystals.